Palaeogeography, Palaeoclimatology, Palaeoecology 540 (2020) 109536

Contents lists available at ScienceDirect

Palaeogeography, Palaeoclimatology, Palaeoecology

journal homepage: www.elsevier.com/locate/palaeo

Boron paleosalinity proxy for deeply buried Paleozoic and Ediacaran fossils

Gregory Retallack

Department of Earth Science, University of Oregon, Eugene, OR 97403-1272, USA

ARTICLE INFO

Keywords:
Dickinsonia
Vendobiont
B/K ratio
Diagenesis
Weaver index

ABSTRACT

Boron content is an indicator of paleosalinity for Mesozoic and Cenozoic clayey sediments, but is compromised by clay diagenesis in deeply-buried sediments of Paleozoic and Ediacaran age. This study of North American, Russian, and Australian, Paleozoic and Ediacaran fossils showed tight covariance of B (ppm) and K (wt%), confirming common wisdom that boron is carried largely by illlite-smectite clays. Ratios of B/K > 40 μg/g distinguish modern marine and freshwater sediments, but this discrimination threshold declines to 21 μg/g for sequences with bituminous coal just below the anchimetamorphic zone, and to 5 μg/g for sequences within the anchimetamorphic zone toward greenschist facies. Marine and non-marine threshold B/K values can be predicted from Weaver and Kübler indices of illite crystallinity, as a measure of B depletion during deep burial and metamorphism. Deviations from that expectation ($\Delta_{B/K\text{-Weaver}}$ and $\Delta_{B/K\text{-Kübler}}$) are positive in marine rocks, and negative in non-marine rocks. Trilobites, stromatolites and other marine fossils were correctly identified as marine by this proxy, and fossil land plants identified as non-marine, though in some cases by small margins because of declining B content with increased clay crystallinity. Cryogenian to Devonian problematic quilted fossils (*Dickinsonia, Arumberia, Rangea, Pteridinium, Ernietta, Aspidella*, *Rutgersella, Protonympha*) are indistinguishable from Devonian to Triassic plants using this proxy, and significantly different from trilobites, brachiopods, ammonites and other securely marine fossils.

1. Introduction

Boron in clays, as a B/K ratio (Walker and Price, 1963), has been used as a paleosalinity proxy because marine waters have higher boron content of 20–50 ppm than about 2 ppm for freshwater (Reynolds, 1965a; Couch, 1971). Unfortunately, diagenetic illitization depletes boron in deeply buried Paleozoic rocks (Spears, 1965; Perry, 1972; Bottomley and Clark, 2004), and metamorphism further exhausts boron (Reynolds, 1965b; Moran et al., 1992; Bebout, 2007). This study explores the boron depletion process with data on boron content and illite crystallinity of deeply buried fossils with the aim of extending the boron paleosalinity proxy to deeply buried Paleozoic and Precambrian rocks. This novel technique can not only be used to confirm paleosalinity of known marine organisms, but also potentially resolve controversy whether Ediacaran vendobionts were marine (Evans et al., 2015; Tarhan et al., 2016, 2017) or freshwater (Retallack, 2013a; Bobkov et al., 2019). Also analyzed were a variety of Precambrian paleosols, in rocks previously regarded as marine (Retallack, 2013a, 2016b, 2018b; Retallack and Mao, 2019).

2. Materials and methods

Some 20–30 g from each specimen were pulverized for aqua regia digestion and ICP-AES analysis of B (10–10,000 ppm range) and melted (670 °C) with sodium peroxide and dissolved in 30% HCl for ICP-AES analysis of K_2O (0.1–30 wt% range) by ALS Geochemistry of North Vancouver, British Columbia (Table 1). Analytical precision (95%) is ± 10 ppm for B and ± 0.13 wt% K_2O. Boron was sometimes below detection limit of 10 ppm, and in those cases the value of x/√2 was used (in this case 7 ppm), the best choice statistically according to Croghan and Egeghy (2003). If there is a bias to this choice over 0 or 5 ppm, the higher value of 7 ppm is a bias toward marine prediction of the boron proxy. Simple weight ratios of B/K (ppm/%, = μg/g) were calculated to normalize for illite content of the matrix, because illite has been shown to be the main carrier of boron in sedimentary rocks (Frederickson and Reynolds, 1960). Literature values cited as B_2O_3 and K_2O were corrected by conversion factors to B (×0.31057) and K (×0.8301).

Thin sections of slabs with impressions of *Dickinsonia costata* and *D. menneri* were point counted (500 points) with a Swift automated stage and Hacker electronic counter, with accuracy of common components of ± 2% (Murphy, 1983). Pulverized rock was plated onto glass slides in deionized water, so that clay platelets were parallel to the slide, and

E-mail address: gregr@uoregon.edu.

https://doi.org/10.1016/j.palaeo.2019.109536
Received 7 December 2019; Received in revised form 11 December 2019; Accepted 12 December 2019
Available online 16 December 2019
0031-0182/

Table 1
Potassium and boron analyses, Weaver (WI) and Kübler (KI) illite crystallinity indices, marine-threshold distance (Δ_{WI} and $\Delta_{KÜ}$), ratio of illite/quartz (10 Å/2.46 Å peaks), XRD-predicted clay (%), and field lithology for selected fossils and paleosols.

Ma	Locality	Formation	Taxon	Condon spem. no.	K %	B ppm	B/K μg/g	WI	Δ_{WI}	KI	Δ_{KI}	Clay/qtz	Clay %	Lithology
242	Summit Lake, B.Col.	Toad Form.	*Gymnotoceras deleeni* (A)	F123765A	0.2	10	50.0	3.4	47	0.44	48	1.57	34	Black shale
248	Newport, NSW	Newport Form.	*Cylostrobus sydneyensis* (P)	F114808	1.4	< 10	5.0	2.5	−25	0.53	−13	1.64	35	Gray shale
248	Avalon, NSW.	Newport Form.	*Cylostrobus sydneyensis* (P)	F105581	1.3	< 10	5.4	2.7	−20	0.53	−13	1.36	33	Gray shale
252	Cararact Dam, NSW.	Wombarra Sh.	*Lepidopteris callipteroides* (P)	F112200A	2.6	< 10	2.7	2.6	−26	0.58	−24	4.58	51	Gray shale
253	Murrays Run, NSW	Wollombi C.M.	*Neomariopteris flexuosa* (P)	F112216	2.3	< 10	3.0	2.7	−22	0.55	−18	3.81	46	Gray shale
257	Yu'xian, China	Shihezi Form.	*Gigantopteris nicotianaefolia* (P)	F112946B	1.5	< 10	4.7	2.9	−12	0.46	−1.3	1.15	32	Green shale
275	Ulladulla, NSW	Ulladulla Mud.	*Notospirifer hillae* (B)	F117280B	1.4	10	7.1	3.3	3	0.44	5	1.15	32	Gray siltstone
306	Tijueras, New Mex.	Los Moyos F.	*Ditomopyge scitulus* (T)	F108679B	1.4	10	7.1	3.2	1.1	0.42	9	1.12	32	Black shale
306	Kostenkovo, Siberia	Alykaev Form.	*Paragondwanidium sibiricum* (P)	F108440C	2.1	< 10	3.3	3.0	−11	0.49	−7	1.54	34	Black shale
308	Petersburg, Indiana	Petersburg F.	*Macroalethopteris scheuzeri* (P)	F106201	2.6	10	3.8	2.9	−12	0.54	−15	1.74	35	Gray shale
318	Bend, Texas	Smithwick F.	*Sevillia trinucleata* (T)	F110201A	0.7	20	28.6	2.7	4	0.42	30	1.33	33	Black shale
330	Cockburnspath, Scot.	Oil Shale	*Sphenopteris affinis* (P)	F106354A	1	10	10.0	2.9	−7	0.51	−4	1.89	36	Oil shale
366	Hyner, Pennsylvania	Duncannon M.	*Rhacophyton ceratangium* (P)	F119212	3.3	< 10	2.1	3.0	−13	0.45	−1.1	1.62	35	Gray shale
381	Naples, New York	Rhinestreet Sh.	*Protonympha salicifolia* (V)	F118356	0.5	< 10	14.0	2.9	−3	0.52	−2	1.19	32	Gray shale
386	Elma, New York	Moscow Form.	*Greenops boothi* (T)	F51458	1.8	20	11.1	3.1	0.3	0.33	26	2.02	37	Gray shale
386	Summit, New York	Moscow Form.	*Protonympha transversa* (V)	F119443	1.4	10	7.1	2.9	−12	0.50	−6	1.27	33	Gray shale
389	Luofu, China	Nandan Form.	*Ductina vietnamica* (T)	F113330A	3.3	10	3.0	3.4	2	0.42	4	2.11	37	Black shale
427	Palmerton, Pennsylv.	Bloomsburg F.	*Nematothallus lobatus* (P)	F116305A	2.3	10	4.3	3.2	−2	0.48	−5	2.64	40	Gray shale
430	North Gates, N.York	Rochester Sh.	*Dalmanites limulurus* (T)	F110412	2.7	20	7.4	3.3	3	0.46	2	1.86	36	Gray shale
437	Delaware Water Gap	Shawangunk F.	*Rutgersella truexi* (V)	F116524A	0.4	< 10	17.5	2.7	−7	0.55	−4	1.08	32	Gray shale
444	Potters Mills, Penns.	Juniata Form.	*Scoyenia beerboweri* (R)	F36203	3.5	10	2.9	3.2	−2	0.47	−5	1.71	35	Red claystone
445	Beans Gap, Tenness.	Juniata Form.	*Lepidotruncus fortis* (P)	F117377C	1.2	10	8.3	3.1	−3	0.48	−1	1.21	32	Red claystone
446	Loysburg, Pennsylv.	Juniata Form.	undescribed (P)	F112810	3.3	10	3.0	3.1	−8	0.46	−3	2.13	37	Gray shale
450	Cincinnati, Ohio	Corryville Mb.	*Flexicalymene meeki* (T)	F108967	3.5	20	5.7	3.3	2	0.42	7	1.78	35	Gray shale
451	Covington, Kentucky	Kope Form.	"Godzillus" (N)	F121265B	1.8	10	5.6	3.3	1.0	0.42	7	1.40	33	Gray shale
453	Swatara Gap, Penns.	Martinsburg F.	*Flexicalymene granulosa* (T)	F106636B	3.4	20	5.9	3.3	3	0.34	20	1.68	35	Gray shale
470	Douglas Dam, Tenn.	Douglas Dam	undescribed (P)	PB2251	4.3	10	2.3	3.0	−10	0.47	−5	1.19	32	Gray shale
472	Ibex, Utah	Fillmore Form.	*Kirkella yersini* (T)	F112980	1.6	20	12.5	3.2	6	0.43	11	1.14	32	Gray shale
475	Florentine Vall., Tas.	Florentine Vall.	undescribed (P)	F123567A	1.7	< 10	4.1	3.0	−9	0.46	−2	1.54	34	Gray shale
495	Trawsffynd, Wales	Cwmshegen F.	*Parabolina spinulosa* (T)	F109879	3.4	10	2.9	3.4	3	0.36	14	2.79	41	Gray shale
504	Wheeler Springs, UT	Wheeler Shale	*Asaphiscus wheeleri* (T)	F106821	2.2	10	4.5	3.4	3	0.41	7	1.75	35	Gray shale
506	Mt Stephen, B.Col.	Burgess Shale	*Anomalocaris canadensis* (X)	F108173	4	10	2.5	3.4	2	0.39	9	2.88	41	Gray shale
510	Cadiz, California	Latham Shale	*Olenellus clarki* (T)	F111543	2.9	20	2.0	3.2	0.2	0.42	7	1.30	33	Gray shale
510	Wirrealpa, S.Aust.	Moodlatana F.	*Erytholus globosus* (V)	F118017B	3.4	20	5.9	3.1	−7	0.47	−0.5	2.40	39	Red claystone
512	Kangaroo Is., S.Aust.	Emu Bay Shale	*Redlichia rex* (T)	F109216B	3.7	20	5.4	3.4	5	0.43	5	2.02	37	Gray shale
515	Qiongzhiusi, Yunnan	Yuanshan Mbr	*Eoredlichia intermedia* (T)	F113071B	3.3	10	3.0	3.4	2	0.41	7	2.38	39	Yellow shale
515	Chengjiang, Yunnan	Yuanshan Mbr	*Cricocosmia jinningensis* (W)	F112959	3.8	10	0.95	3.4	0.5	0.41	6	1.73	35	Gray shale
533	Lava River, Russia	Lontova Form.	Janischevskyites petropolitanus (F)	F108652	4.7	40	8.5	3.2	1.4	0.39	15	2.53	40	Green shale
533	Tosna River, Russia	Lontova Form.	*Platysolenites antiquissimus* (F)	F108965	4.5	40	8.9	3.2	0.7	0.38	16	2.38	39	Green shale
539	Fishtrap Lake, Mont.	Flathead Sand.	undescribed (V)	F113717B	2.9	10	3.4	3.0	−11	0.48	−5	1.95	36	Red claystone
541	Parachilna G., S·Au.	Parachilna F.	*Skolithos linearis* (R)	R3299	2.1	10	4.8	3.4	4	0.43	5	1.14	32	Red claystone
541	Swartpunt, Namibia	Spitzkopf Mbr	*Manykodes pedum* (R)	F120826	0.5	10	20.0	3.1	9	0.38	27	1.34	33	Gray siltstone
543	Tecopa, California	Wood Canyon	*Ernietta plateauensis* (V)	F123791A	1.3	10	7.7	3.1	−4	0.50	−4	1.14	32	Gray siltstone
543	Tecopa, California	Wood Canyon	undescribed (V)	F123788	1.9	< 10	3.7	3.0	−11	0.46	−2	1.09	32	Gray shale
545	Mt Dunfee, Nevada	Esmeralda Mbr	*Elainabella deepspringensis* (L)	F123797A	1.6	10	6.3	3.4	4	0.43	6	2.74	41	Gray shale
545	Mt Dunfee, Nevada	Esmeralda Mbr	*Conotubus hemiannulatus* (W)	F123798	3.6	10	2.8	3.4	1.1	0.44	0.7	1.13	32	Gray shale
546	Swartpunt, Namibia	Feldshuhorn M.	*Pteridinium carolinaense* (V)	F120823B	1.7	< 10	4.1	2.9	−12	0.48	−4	1.58	34	Green siltstone
546	Swartpunt, Namibia	Feldshuhorn M.	*Ernietta plateauensis* (V)	F120825B	2.4	< 10	2.9	2.9	−15	0.48	−6	2.74	41	Green siltstone
547	Jiulongwan, China	Shibantan Mbr	*Lamonte trevallis* (I)	F117748A	0.1	< 10	70.0	2.8	49	0.44	68	1.07	32	Limestone
548	Ernietta Hill, Namib.	Aar Member	*Rangea scheiderhoehni* (V)	F120812	0.5	< 10	14.0	2.8	−6	0.51	−0.3	1.11	32	Gray siltstone
549	Aarhausen, Namibia	Mooifontein M.	*Beltanelliformis brunsae* (D)	F120803	0.3	< 10	23.3	2.9	6	0.45	19	1.12	32	Gray siltstone
550	Brachina G., Aust.	Ediacara Mbr	Yaldati paleosol (S)	R3206	1.7	10	5.9	3.2	−2	0.49	−4	1.32	33	Red siltstone
550	Ross River, N.Territ.	Arumbera Sst.	undescribed (V)	F117264	2.6	10	3.8	3.2	−3	0.46	−1.0	1.39	33	Red siltstone

(*continued on next page*)

Table 1 (*continued*)

Ma	Locality	Formation	Taxon	Condon spem. no.	K %	B ppm	B/K μg/g	WI	Δ_{WI}	KI	Δ_{KI}	Clay/qtz	Clay %	Lithology
550	Pockenbank, Namib.	Kanies Member	*Ernietta plateauensis* (V)	F120819	3.6	< 10	1.9	2.7	−22	0.49	−8	1.26	33	Red siltstone
550	Brachina G., Aust.	Ediacara Mbr	*Dickinsonia costata* (V)	F115737	1.7	< 10	4.1	3.2	−3	0.46	−0.7	1.32	33	Red siltstone
550	Luga bore, Russia	Kostov Form.	*Vendotaenia antiqua* (L)	F108650B	3.5	40	8.5	3.2	0.6	0.43	8	2.15	37	Green shale
555	Zimnie Gory, Russia	Erga Formation	*Dickinsonia menneri* (V)	F123776U	2.1	10	4.8	2.9	−13	0.53	−11	1.28	33	Green siltstone
555	Zimnie Gory, Russia	Erga Formation	*Dickinsonia menneri* (V)	F123776M	2	10	5.0	2.9	−12	0.52	−11	1.28	33	Green siltstone
555	Zimnie Gory, Russia	Erga Formation	*Dickinsonia menneri* (V)	F123776L	2	10	5.0	2.9	−12	0.52	−11	1.28	33	Green siltstone
558	Altar Stones, UK	Bradgate Form.	*Cyclomedusa davidi* (D)	F116160	1.2	< 10	5.8	3.4	5	0.38	14	2.57	40	Gray siltstone
560	Centr. Mt. Stuart, NT	Grant Bluff F.	*Arumberia banksi* (V)	F119657A	1.5	< 10	4.7	2.8	−17	0.50	−7	1.52	34	Red siltstone
560	Ferryland, Newfld	Fermeuse F.	*Aspidella terranovica* (V)	F116773	2.6	10	3.8	3.1	−6	0.47	−4	3.26	43	Black shale
560	Novodniestrovsk, Uk	Lomosov Bed	*Beltanelliformis brunsae* (D)	F115777	3.2	10	3.1	2.9	−13	0.45	−1.2	1.28	33	Green shale
565	Mistaken Point, Nfld	Mistaken Point	*Aspidella terranovica* (V)	F116787	2.8	10	3.6	3.1	−7	0.46	−1.4	2.49	39	Green siltstone
565	Tecopa, California	Stirling Quartz.	undescribed (D)	F123782A	3.8	10	3.7	3.1	−10	0.48	−6	1.75	35	Gray siltstone
567	Bunyeroo G., S·Au.	Wonoka Form.	*Palaeopascichnus delicatus* (R)	F115701	2.6	10	3.8	3.4	3	0.34	19	1.86	36	Gray shale
580	Tecopa, California	Johnnie Form.	*Boxonia pertaknurra* (O)	F123779A	0.6	10	16.7	3.3	11	0.39	30	1.52	34	Limestone
580	Hewitts Cove, Mass.	Cambridge Ar.	*Aspidella terranovica* (V)	F114496	2.4	< 10	2.9	3.2	−3	0.48	−6	1.57	34	Gray siltstone
700	Pocatello, Idaho	Scout Mountain	undescribed. (V)	F123473	2.5	< 10	2.8	3.1	−8	0.50	−9	1.80	36	Gray siltstone
700	Pocatello, Idaho	Scout Mountain	undescribed (D)	F121216	1.9	< 10	3.7	3.1	−7	0.50	−8	2.02	37	Gray siltstone
750	Red Pine Creek, UT	Red Pine Shale	undescribed (M)	F118773B	1.2	10	8.3	3.0	−8	0.51	−5	1.52	34	Limestone
1000	Allamore, Texas	Allamore Fm.	*Conophyton concellosum* (O)	F108092A	0.2	20	100	3.3	97	0.47	92	1.05	32	Limestone
1000	Horsethief Spr., CA	Beck Spr. Dol.	*Tenuocharta cloudii* (L)	F116630A	0.1	10	100	3.3	96	0.45	96	1.04	31	Gray chert
1325	Deep Creek, MT	Greyson Shale	*Grypania spiralis* (L)	F115996A	3.1	20	6.5	3.3	2	0.41	9	1.60	34	Gray shale
1450	Neihart, MT	Chamberlain	*Lanceoforma striata* (L)	F115985B	0.8	20	25.0	3.3	21	0.41	27	1.26	33	Gray shale
1480	Appekunny Mt., MT.	Appekunny Sc.	*Horodyskia moniliformis* (G)	F116015A	2.5	10	4.0	3.1	−7	0.47	−2	1.42	33	Green shale
1500	Appekunny Mt., MT	Altyn Limest.	*Collenia columnaris* (O)	F121570	0.3	10	33.3	3.3	28	0.30	54	1.88	36	Limestone
1700	Daheitan, China	Yungmenshan	Hougou paleosol (Z)	R5586	0.2	< 10	35.0	3.4	33	0.48	26	1.04	31	Gray siltstone
1800	Stirling Range, WA.	Stirling Range	*Cyclomedusa davidi* (D)	F116402	0.9	< 10	7.8	3.0	−6	0.49	−3	1.35	33	Red siltstone
1800	Stirling Range, WA.	Stirling Range	*Cyclomedusa davidi* (D)	F116400	1.2	10	8.3	3.0	−5	0.49	−2	1.21	32	Red siltstone
2200	Waterval Onder, Afr.	Hekpoort Bas.	*Diskagma buttonii* (S)	F116533A	7.1	< 10	1.0	3.3	−3	0.46	−4	7.52	66	Green schist
3000	Mt Grant, WA	Farrel Quartzite	Jurl paleosol (Z)	R4348	0.3	< 10	23.3	3.4	22	0.40	28	3.33	44	Black chert
3255	Strelley Gorge, WA.	Leiliria Form.	Jurl paleosol (Z)	R4328	0.9	< 10	7.8	3.4	5	0.37	16	1.10	32	Black chert
3420	Marble Bar, WA.	Double Bar F.	Kartu paleosol (S)	R4204	2.5	10	2.9	3.3	−1.3	0.47	−3.8	1.39	33	Green schist
3420	Marble Bar, WA.	Apex Chert	Kartu paleosol (S)	R3786	2.4	< 10	4.0	3.2	−1.9	0.46	−1.4	2.16	37	Green schist
3460	Panorama Port., WA.	Panorama F.	Jurl paleosol (Z)	R3756	0.3	< 10	23.3	3.3	20	0.36	35	1.04	31	Black chert
3465	Marble Bar, WA	Apex Chert	*Eoleptonema apex* (C)	F117673	0.1	< 10	70	3.4	70	0.28	94	1.10	32	Black chert
3700	Isukasia, Greenland	Isua Supracr.	Isi paleosol (Z)	R5312	0.01	< 10	700	3.4	699	0.26	728	1.17	32	Black schist

Codes in taxon column: (A) ammonite, (B) brachiopod, (C) prokaryotic microfossils, (D) discoid microbial colony, (F) foraminifera, (G) glomeromycotan fungus, (I) slime mold, (L) algae, (M) amoebozoan, (N) cnidarian, (O) stromatolite, (P) plant, (R) trace fossil, (S) non-crystic paleosol, (T) trilobite, (V) vendobiont, (W) worm, (X) anomalocarid arthropod, (Z) crystic playa paleosol. All specimens in Condon Collection (online catalog paleo.uoregon.edu).

Table 2
Threshold marine B/K mass ratio, Weaver and Kübler indices of illite crystallinity.

Geological Age	Location	Threshold B/K (μg/g)	Weaver index	Kübler index	Reference
Holocene	Lake Superior, USA	40	2.1	0.65	Nussman, 1965, Goldberg and Arrhenius (1958), Jeong and McDowell (2003),
Cretaceous	Austria	52	1.9	0.75	Hofer, 2009
Carboniferous	Yorkshire, UK	21	2.8	0.60	Spears (1965), Spears and Sezgin (1985)
Carboniferous	Donbass, Ukraine	16	3.0	0.52	Środoń and Paszkowski (2011)
Ediacaran	Brachina Gorge, S. Australia	5	3.2	0.40	Retallack, 2013a

then scanned using a Rigaku x-ray diffractometer with Cu−Ni radiation in the Department of Earth Sciences, University of Oregon, Eugene, with data extracted using a FORTRAN program written for this purpose by M.H. Reed. These traces were used to calculate two crystallinity indices: Weaver index (10 Å/10.5 Å peak height, = height at 8.84/8.42 °2θ) and Kübler index (width at half height of 10 Å peak in °2θ). Kübler indices were not standardized as recommended by Warr and Ferreiro Mählmann (2015), because source diffractograms from literature compilation were not standardized (Table 2; Spears and Sezgin, 1985; Jeong and McDowell, 2003; Hofer, 2009, Środoń and Paszkowski, 2011). As suspected by the need for standardization, Kübler index was found to be less reliable than Weaver index. Weber index is a third popular crystallinity index (Frey, 1987), but was not calculated because the same source diffractograms used for calibration did not all extend to quartz peaks.

Analyses were performed on the shale or siltstone matrix of well-lithified to metamorphosed fossils and paleosols, ranging in age from 242 to 3700 million years old (Table 1). Sample selection was guided for comparability with Ediacaran vendobiont fossils, which are in the anchimetamorphic zone of burial alteration, approaching greenschist and prehnite-pumpellyite metamorphic facies (Retallack, 2013a, 2016b). Point count data on mineral modes is published for 12 of the 88 specimens analyzed (F36203 = R176, F112810 = R2297, F113717= F3595, F115737, F116787 = R4003, R116400 = R3839, F125776, R3206, R3756, R3786, R4204, R4348 from Retallack, 2001, 2012, 2013b, 2015b, 2016b, 2018b, Retallack et al., 2013a, 2016; Retallack and Mao, 2019). These have 35 ± 5% clay (one standard deviation), and a surprising 45 ± 14% silt. These 12 point-counts were used as a training set to predict the clay abundance and clay:quartz ratio of all 88 specimens (Table 1), following the recommendation of Fisher and Underwood (1995) of linear regression from ratios of the 10 Å peak for illite and the 2.46 Å peak for quartz on X-ray diffractograms (Fig. 1). The abundance of silt in early Paleozoic and Ediacaran shales has been noted before, and blamed on widespread windblown dust before the advent of land plants (Dalrymple et al., 1985; Retallack, 2012, 2013a, 2019).

Only the silicate matrix was analyzed, not shell nor carapace, of *Anomalocaris*, trilobites, brachiopods, and foraminifera. Vendobionts are a group of problematic quilted fossils best known from rocks of Ediacaran age (Seilacher, 1992), but also recognized now in Cambrian through Devonian rocks (Retallack, 2008, 2013b, 2018a), and perhaps as old as Cryogenian (Keeley et al., 2013). Casts of the upper surface (*Dickinsonia* of Table 1) were analyzed, as well as internal fills of some vendobionts (*Arumberia, Ernietta*, *Rangea*, *Pteridinium*, *Erytholus* of Table 1). *Aspidella* is here included with vendobionts rather than discoids, because type material has small quilts within the apex, and oriented specimens show that attached tubular features are rhizomorphs (Retallack, 2016b), rather than frond stalks (Gehling et al., 2000). Undescribed problematic fossils included reticulate markings from Fishtrap Lake Montana (Retallack, 2013b), and from Pocatello, Idaho (Keeley et al., 2013). Some analyzed Ordovician plants were illustrated by Retallack (2000, 2001), but others are undescribed, with details available online (paleo.uoregon.edu). Undescribed Tonian thecamoebians are similar to those described by Porter et al. (2003), but in shale rather than nodules. Trace fossils like those of dictyostelid slime molds include *Lamonte trevallis* from the Shibantan Member of China, and *Myxomitodes stirlingensis* from the Western Australian Stirling Range Formation (Retallack and Mao, 2019). Non-saline paleosols analyzed range in age from Ordovician to Paleoarchean (442–3420 Ma) and are described fully elsewhere (Retallack, 2013a, 2013b, 2015a, 2015b, 2016b, 2018b). Acid-sulfate paleosols with abundant sand crystals, also known as playa evaporites, were separated as a distinct category that is exceptionally boron-rich (Retallack et al., 2016; Retallack, 2018a; Retallack and Noffke, 2019; Retallack and Mao, 2019). All specimens are curated in the Condon Collection of the Museum of Natural and Cultural History of the University of Oregon (online portal paleo.uoregon.edu).

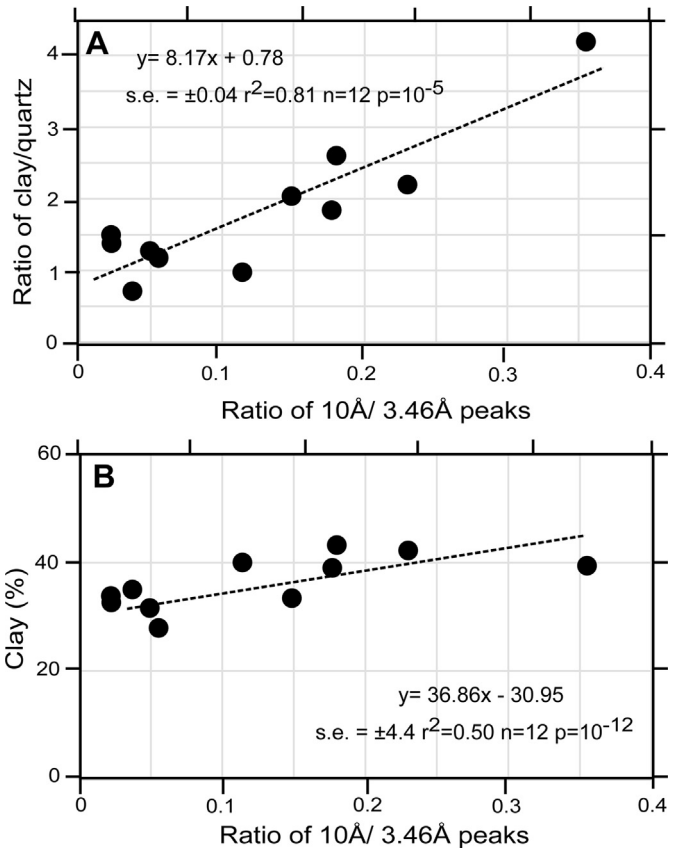

Fig. 1. Prediction of the ratio of clay/quartz (A) and percent clay (B) from 12 of the analyzed specimens using the ratio of illite (10 Å) and quartz (3.46 Å) peaks in X-ray diffractograms.

3. Paleosalinity from B/K ratios at different diagenetic alteration grades

The boron paleosalinity proxy is based on the observation that marine waters have higher boron content (20–50 ppm) than freshwater (ca. 2 ppm), and comparable differences are preserved in clays, especially illites (Frederickson and Reynolds, 1960; Couch, 1971). Thus, B/

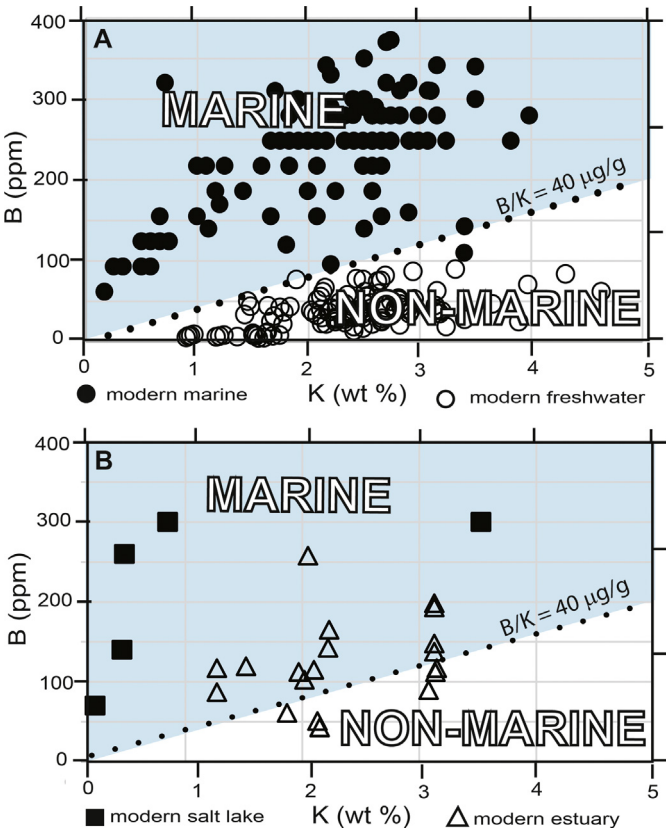

Fig. 2. B/K mass ratios (µg/g) of modern marine versus lakes and rivers (A) and of estuaries and saline lakes (B). Data for A from Goldberg and Arrhenius (1958), Ericson et al. (1961), Nussman (1965), Mackereth (1966), Chetelat et al. (2009), and Ercolani (2018). Data for for B from Shirodkar and Dalal (1988), and Wei et al. (2014).

K ratios can be used to discriminate marine and nonmarine sediments (Walker and Price, 1963; Reynolds, 1965a). This approach became less popular when it was discovered that diagenetic illitization depletes boron in Paleozoic rocks (Spears, 1965; Perry, 1972; Bottomley and Clark, 2004), and metamorphism further depletes boron (Reynolds, 1965b; Moran et al., 1992; Bebout, 2007). Thus other element ratios for paleosalinity, such as B/Ga, have proven more popular (Ye et al., 2016; Wei et al., 2018).

A new compilation of published data on modern sediments, shows that a B/K ratio of 40 µg/g discriminates marine from nonmarine (Fig. 2A), including those of rivers (Chetelat et al., 2009; Ercolani, 2018), lakes (Nussman, 1965; Mackereth, 1966), and the ocean (Goldberg and Arrhenius, 1958; Ericson et al., 1961). Data on river and lake sediments were completely fresh water, and data on marine sediments from deep sea cores and dredges, so that these form end members. These data are also B contents of bulk sediment, not separated clays, as recommended for B-paleosalinity work in the past (Walker and Price, 1963). Clay separation is problematic at high grades of diagenetic and metamorphic recrystallization of clays (Frey, 1987). As expected, estuarine sediments (Shirodkar and Dalal, 1988) have values straddling 40 µg/g, and acid sulfate lake (playa or Gypsid soil) sediments have exceptionally high boron (Fig. 2B). Concentration of boron in playas is so extreme as to form boron ores, such as ulexite, and this kind of paleosol differs from others in obvious salt crystals and sand crystals (Kistler and Helvaci, 1994; Wei et al., 2014).

In buried and diagenetically altered sedimentary rocks, such as interbedded fossiliferous marine shales and non-marine underclays to bituminous coals of Carboniferous cyclothems in Yorkshire (Spears, 1965), a B/K ratio of 21 µg/g separates marine from non-marine (Fig. 3). Two other cases of interbedded marine and non-marine rocks

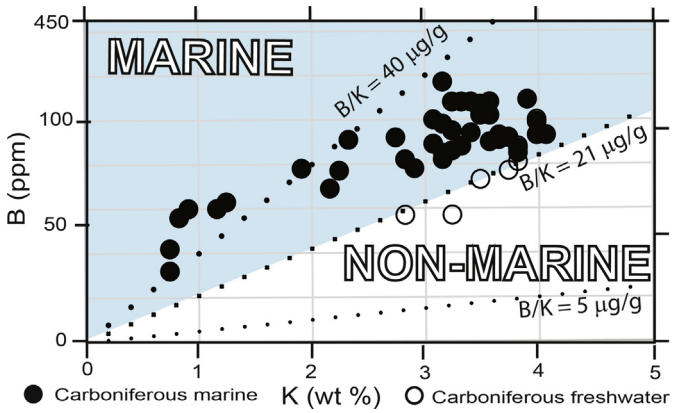

Fig. 3. B/K mass ratios (µg/g) of Carboniferous marine versus non-marine claystones in the Yoredale Series (Westphalian) of Yorkshire UK (data from Spears, 1965).

(Hofer, 2009; Środoń and Paszkowski, 2011) together with data on illite crystallinity (Table 2) from Weaver and Kübler indices (from diffractograms of Spears and Sezgin, 1985; Jeong and McDowell, 2003) reveal a significant relationship between the marine and non-marine threshold value of B/K. As the Weaver index increases and the Kübler index decreases with heat and pressure, the 10 Å peak of illite becomes sharper and narrower, recrystallizing by Ostwald ripening, and expelling boron (Fig. 4). A recrystallization mechanism has also been used to explain $\delta^{11}B$ and $\delta^{18}O$ changes in shales with burial (Ishikawa and Nakamura, 1993; Williams et al., 2001; Williams and Hervig, 2005). Thus, the expected threshold values (B/K_{Weaver} and $B/K_{Kübler}$) between marine and non-marine B/K ratio in µg/g can be predicted from Weaver index (W) and Kübler index ($\ddot{U}$) of the 10 Å peak of illite (Fig. 5). Divergence of an individual sample from that predicted threshold value can be expressed using delta (Δ) notation, as follows

$$B/K_{Weaver} = -32.55W + 112 \quad (1)$$

$$B/K_{Kübler} = 164.67\ddot{U} - 70.25 \quad (2)$$

$$\Delta_{B/K-Weaver} = B/K_{sample} - B/K_{Weaver} \quad (3)$$

$$\Delta_{B/K-Kübler} = B/K_{sample} - B/K_{Kübler} \quad (4)$$

Eq. (1) has r^2 of 0.98, standard error of ± 2.9, $n = 4$, and probability of 10^{-5}. Eq. (2) has r^2 of 0.98, standard error of ± 3.0, n = 4, and probability of 10^{-5}. In the case of $\Delta_{B/K}$, positive numbers are marine and negative values are non-marine. Most samples chosen for this study were depleted in boron because they suffered burial temperatures of 200–300 °C and pressures of 2–4 kbar (Frey, 1987), so that $\Delta_{B/K}$ is a more reliable paleosalinity proxy than B/K. The high correlation of Eqs. (1) and (2) was surprising, but is from only four points of metadata from literature survey. Ediacaran data presented here was colinear (Fig. 5), but not included in Eqs. (1) and (2) so the Ediacaran could be independently evaluated. These relationships deserve wider testing to embrace likely variability of the relationship between boron content and crystallinity of clays.

Recommended procedure for determining paleosalinity from boron thus requires three independent numbers, one each of B (ppm) and K (wt%), and either the Weaver or Kübler index of the illite 10 Å peak from an XRD trace. These are then converted to $\Delta_{B/K}$ (Eqs. (3) or (4)), which can be above the marine-non-marine threshold of 0, and thus marine, or below it, and thus non-marine. The standard error of prediction is ± 2.9 $\Delta_{B/K}$, and 22 of 88 fossils analyzed fall within ± 2.9 $\Delta_{B/K}$, so are insecurely assigned (Table 1). Insecure assignment to marine or non-marine within ± 2.9 $\Delta_{B/K}$ is not a failure of the technique, but more likely an indication of mixed lagoonal or estuarine salinities. Although results from both Weaver and Kübler indices turned out to be comparable, Weaver index is preferred, because more significant

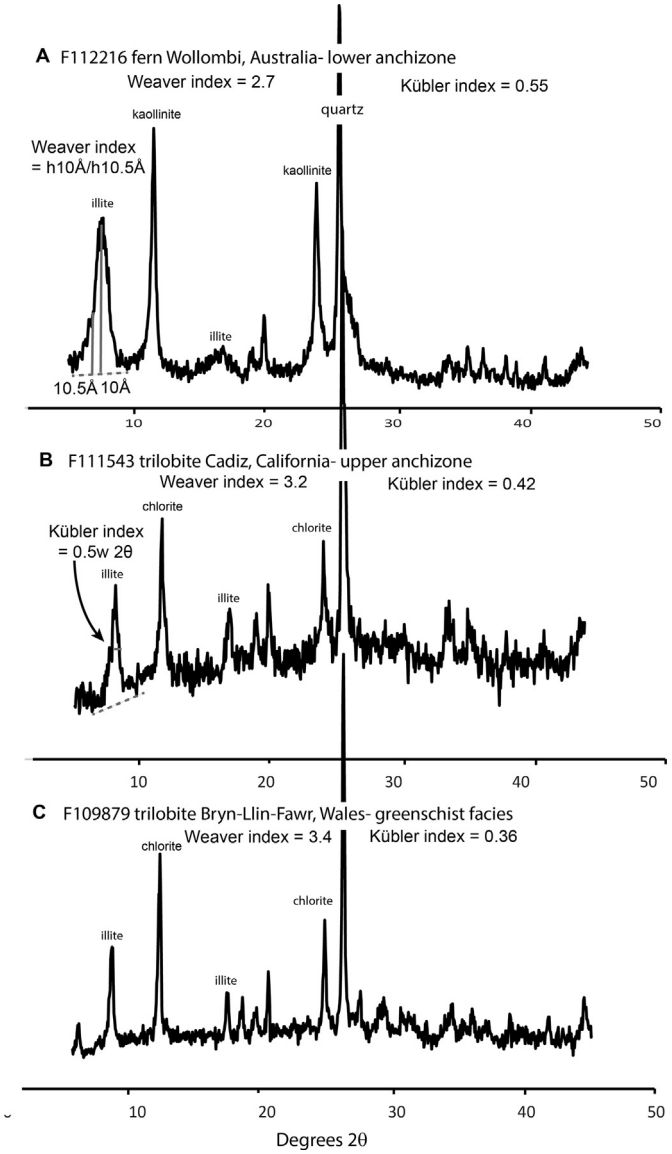

Fig. 4. Example X-ray diffractograms showing narrowing of the 10 Å (=8.82 °2θ) peak with higher grade diagenesis and metamorphism.

figures allow greater precision. Furthermore, the Kübler index sometimes returns implausible negative B/K threshold values, perhaps in part because not standardized (Warr and Ferreiro Mählmann, 2015).

4. General survey results

4.1. Boron assay overview

Six general groups of fossils are contrasted in Table 3 and Fig. 6: (1) unequivocally marine trilobites, ammonites, brachiopods, and foraminifera, (2) unequivocally non-marine fossil plants, (3) non-saline paleosols, (4) playa paleosols with sand crystals, (5) problematic vendobionts, and (6) enigmatic discoid fossils. Vendobionts are not statistically distinct from plants in $\Delta_{B/K\ Weaver}$ (*t*-test $p = 0.06$), but vendobionts and marine fossils are very distinct ($p = 10^{-4}$), and so are plants and marine fossils ($p = 10^{-5}$).

The highest boron values were found in the playa paleosols, which are thus similar to modern acid-sulfate lakes with boron minerals (Fig. 2B: Kistler and Helvaci, 1994; Wei et al., 2014). This kind of paleosol with abundant sulfate sand crystals is very common in Archean rocks (Retallack et al., 2016; Retallack, 2018a), and may include the

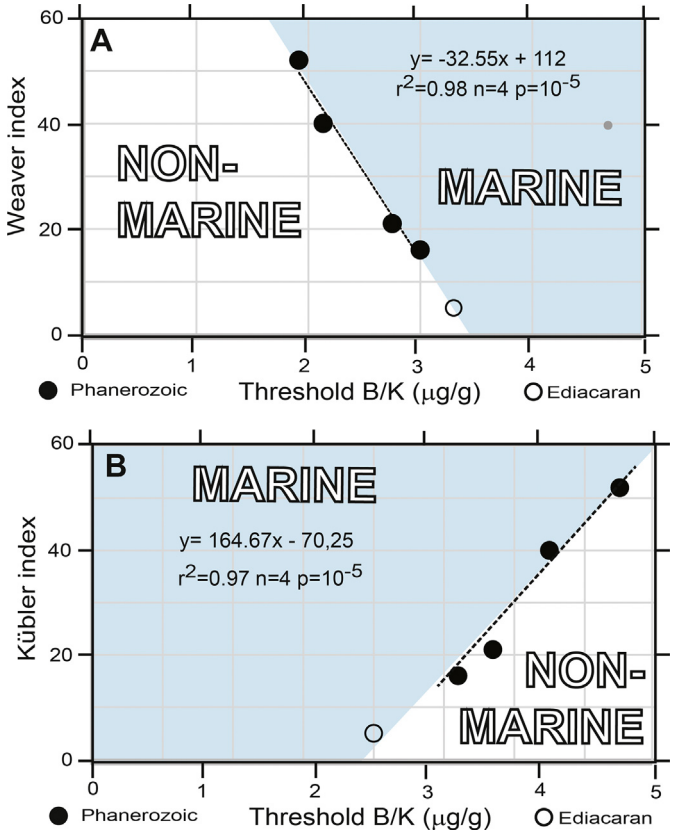

Fig. 5. Threshold marine/non-marine B/K mass ratios (μg/g) predicted by Weaver index (A) and Kübler index (B) of illite crystallinity (data in Table 2).

oldest paleosol known (Retallack and Noffke, 2019). High positive values in unequivocal marine fossils and low negative values in fossil plants are also not surprising. Enigmatic discoid fossils straddle the marine-non-marine threshold, with some of them marine and some non-marine. Vendobionts were consistently negative for $\Delta_{B/K}$, and thus non-marine. This is true for vendobionts found in what has been regarded as marine facies of the Cambridge Argillite of Massachusetts (Thompson et al., 2014), intertidal facies of the Fermeuse Formation of Newfoundland (Retallack, 2016b), and Flathead Sandstone of Montana (Retallack, 2013b), in estuarine facies of the Shawangunk Sandstone of New Jersey (Retallack, 2015a), and coastal lagoon facies of the Moscow Formation and Rhinestreet Shale of New York (Retallack, 2018a), as well as those in fluvial-eolian facies of the Ediacara Member in South Australia (Retallack, 2013a) and the Kanies Member in Namibia (Retallack, 2019). The Feldshuhorn Member at Swartpunt in Namibia is a poorly fossiliferous green siltstone without paleosols, stratigraphically below the abundant trace fossils at Swartpunt (Darroch et al., 2015), and may have been a coastal lagoon. Some vendobionts were found in pyritic intertidal paleosols like those that now support salt marsh and mangal vegetation (Retallack, 2016b), but still had freshwater boron content. Vendobionts may have been primarily non-marine to estuarine.

Different discoid fossils are marine and non-marine, compatible with interpretation as microbial colonies (Grazhdankin and Gerdes, 2007). Discoid fossils from the Mooifontein Member in Namibia were found to have been marine, and as also apparent from occurrence in a thin sandstone band within limestones crowded with *Cloudina* and other shelly fossils (Hall et al., 2013). Similarly, the large pyrite nodules in matrix below discoid fossils from the Bradgate Formation of England (Table 1), are comparable with intertidal anoxic paleosols (Retallack, 2013b). Comparable discoid fossils have been interpreted in the past as sea jelly medusae, which are found both in modern lakes and oceans

Table 3
B/K mass ratios (μg/g) and departure from crystallinity-predicted marine-thresholds.

Group	Number of analyses	B/K (μg/g)	$\Delta_{B/K\text{-Weaver}}$ (μg/g)	$\Delta_{B/K\text{-Kübler}}$ (μg/g)
Marine fossils	22	14.8 ± 21.9	9.8 ± 9.9	18.6 ± 21.3
Plant fossils	12	4.1 ± 2.0	−13.5 ± 7.4	−8.4 ± 7.3
Non-saline paleosols	6	4.1 ± 2.6	−2.4 ± 0.9	−3.1 ± 1.7
Playa paleosols	4	188.6 ± 341.0	155.8 ± 303.8	166.6 ± 314.0
Vendobionts	20	5.9 ± 4.2	−9.3 ± 5.2	−4.8 ± 3.4
Discoids	7	7.8 ± 7.2	−4.4 ± 7.1	−1.0 ± 2.7

(Fritz et al., 2007), but the fossils lack any distinctive cnidarian features (Seilacher, 1992). The other discoid fossils studied are all non-marine in boron content, including fossils atop paleosols from the Stirling Range of Western Australia (Retallack and Mao, 2019), like those reported from Precambrian "desiccated facies" by Grazhdankin et al. (2012).

4.2. Individual problematic cases

The paleosalinity of other fossils determined here may aid in their interpretation. For example, some Cambrian examples of the trace fossil *Skolithos* in the Wood Canyon Formation of California have been considered non-marine (Kennedy and Droser, 2011), and this study confirms that other fossils from that formation and the underling Stirling Quartzite were nonmarine. In contrast, Cambrian *Skolithos* associated with *Diplocraterion* from an intertidal paleosol (Madla pedotype) in the Parachilna Formation in South Australia was marine (Retallack, 2008). These distinctive metazoan burrows are mainly marine, but their makers may have invaded estuaries.

Unsurprising is high boron as evidence of marine habitat for putative algae *Elainabella* (Rowland and Rodriguez, 2014), *Vendotaenia* (Hofmann, 1985), *Tenuocharta* (Horodyski and Mankiewicz, 1990), *Grypania*, and *Lanceoforma* (Walter et al., 1976), and the trace fossil *Manykodes* (Retallack, 2013b). *Manykodes pedum* (Dzik, 2005) is sometimes still called "*Treptichnus pedum*" (Buatois and Mángano, 2016), but *Treptichnus* is found in Pennsylvanian freshwater shales, and has much straighter segments than *Manykodes* (Rindsberg and Kopaska-Merkel, 2005). Also unsurprising is low boron as evidence of freshwater for *Diskagma* in a vertic paleosol (Retallack et al., 2013a), and for Precambrian thecamoebans, although these particular thecamoebans are in intertidal facies of the Red Pine Shale (Dehler et al., 2010). All living thecamoebans are soil protists (Porter et al., 2003). Proterozoic *Horodyskia* (Retallack et al., 2013b) also have been considered marine, but have freshwater boron contents for their metamorphic grade. *Lamonte* has been considered a marine worm burrow (Meyer et al., 2014), and does have marine boron levels, but may be a slime mold grex of supratidal flats (Retallack and Mao, 2019). The problematic fossils *Palaeopascichnus* (Antcliffe et al., 2011) and *Conotubus* (Smith et al., 2016) also appear to have been marine.

5. Case study of Ediacaran *Dickinsonia*

5.1. Geological background

Dickinsonia is an iconic example of the Vendobionta (Fig. 7), and the center of controversy whether it was marine (Evans et al., 2015; Tarhan et al., 2016, 2017) or freshwater (Retallack, 2013a; Bobkov et al., 2019). The specimen of *Dickinsonia costata* analyzed (Fig. 87A) was from the Ediacara Member of the Rawnsley Quartzite in Brachina Gorge, South Australia (32 m in the section of Retallack, 2013a). The specimen of *Dickinsonia menneri* (Fig. 7B) was from the Erga Formation at Zimnie Gory, north of Arkhangelsk, Russia (368 m in the section of Grazhdankin, 2004). The South Australian Rawnsley Quartzite overlies the fluvial Bonney Sandstone with paleosols, and underlies shallow marine Uratanna Formation with Cambrian trace fossils *Manykodes*

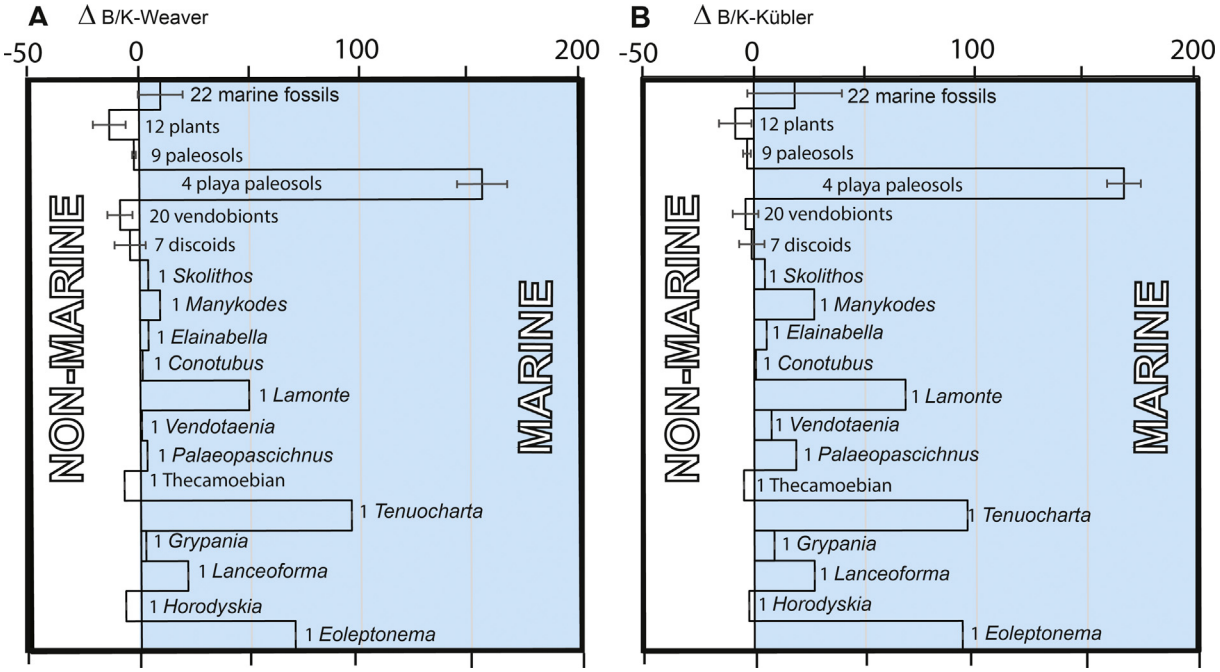

Fig. 6. Marine to non-marine thresholds normalized for illite crystallinity calibration of diagenetic and metamorphic alteration, using two separate metrics, $\Delta_{B/K\ Weaver}$ (A) and $\Delta_{B/K\ Kübler}$ (B).

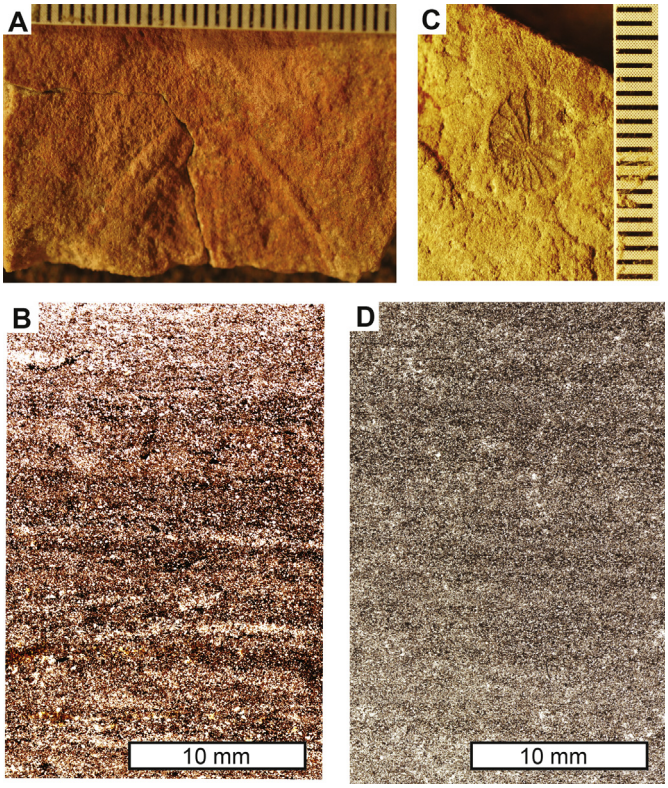

Fig. 7. Analyzed specimens of *Dickinsonia costata* (A) from South Australia and *D. menneri* (B) from northwestern Russia, with thin sections of their matrix (B and D).

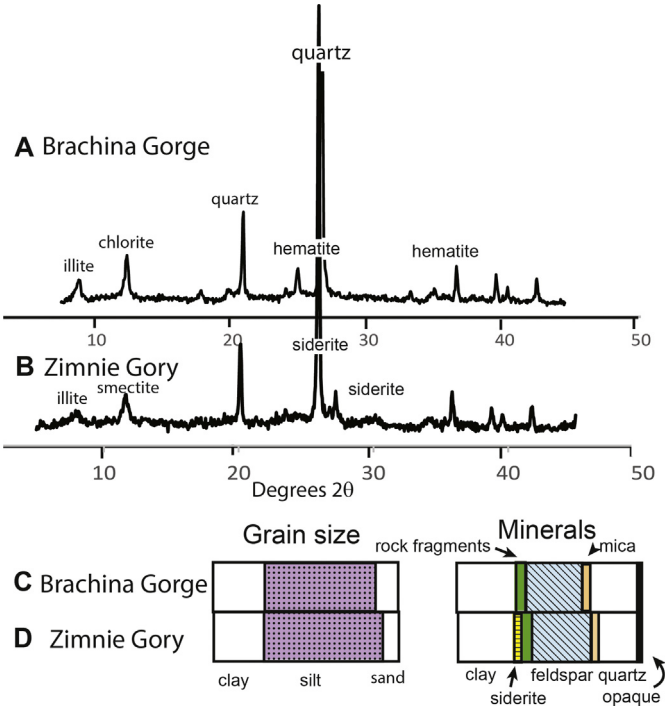

Fig. 8. X-ray diffractograms (A–B) and petrographic composition (C–D) of *Dickinsonia* illustrated in Fig. 7.

pedum (Retallack et al., 2014). The Russian Erga Formation is within an epicontinental, deltaic and offshore siliciclastic sequence overlying a 40-m-thick Oxisol paleosol developed on Mesoproterozoic metamorphic basement (Grazhdankin and Bronnikov, 1997; Liivamägi et al., 2014, 2015).

Both *Dickinsonia* specimens are negative hyporeliefs, or impressions in the sandstone layer directly overlying the original fossil. In thin section, they are similar in bundled thin laminations, and dominance by silt-sized grains (Fig. 8C–D), which can be taken as evidence of eolian deposition (Retallack, 2012). Point counting also revealed similarities in silt content (53.6% in South Australia and 59.6% in Russia), K-feldspar (27.6% in South Australia and 31.0% in Russia), and quartz (25.5% in South Australia and 24.8% in Russia) content (Fig. 8C, D). Detrital mica did not include muscovite, but chlorite and biotite are 6.6% in South Australia and 2.4% in Russia. The main differences between the two matrices are red color and abundant hematite of the South Australian specimen (Figs. 7A, 8C), but gray color and siderite grains of the Russian specimen (Figs. 7C, 8D). South Australian *Dickinsonia* has well crystallized illite and chlorite (Fig. 8A), low in the greenschist metamorphic facies, due to burial by 6 km (Retallack, 2013a). In contrast, poorly crystallized illite-smectite in Russian *Dickinsonia* (Fig. 8B), supported by low thermal maturity of organic matter (Pehr et al., 2018), isopachs (Maslov et al., 2009), and diagenetic illite polytypes (Gorokhov et al., 2005), are evidence for burial by no > 2 km of overburden. There is no evidence of hydrothermal alteration, such as veining, brecciation, or ore minerals, on these specimens (Fig. 7B, D). Recrystallization of illite in the South Australian specimens was a solid solution, Ostwald ripening process (Novoselov and de Souza Filho, 2015), because tau analysis of beds there shows depletion of potassium preserved from soil formation (Retallack, 2012).

Neither the Russian nor Australian fossils show surface oxidation rinds (Fig. 7A, C). Both are from little-weathered outcrops, in a sea cliff in the case of the Russian specimen (Grazhdankin, 2004), and in a steep gorge of the most seismically active region of South Australia (Retallack, 2012, 2013a). Both also were found in rocks that become marine a few hundred meters higher in the sequence (Pirrus, 1992; Retallack et al., 2014). Matrix to those marine fossils was analyzed as a test for systematic boron deficiencies in source areas, and such deficiency was not found (Table 1).

5.2. Boron assay of Dickinsonia

Results for *Dickinsonia menneri* are compared with known marine fossils from the same general sequence (Fig. 9), such as the Cambrian foraminifera, *Yanischevskyites petropolitanus* and *Platysolenites antiquissimus* (McIlroy et al., 2001), and the Ediacaran seaweed, *Vendotaenia antiqua* (Hofmann, 1985) in northwestern Russia (Table 1). Also compared are Cambrian (Mindi and Madla pedotypes) and Ediacaran (Yaldati pedotype) paleosols from South Australia (Retallack, 2008,

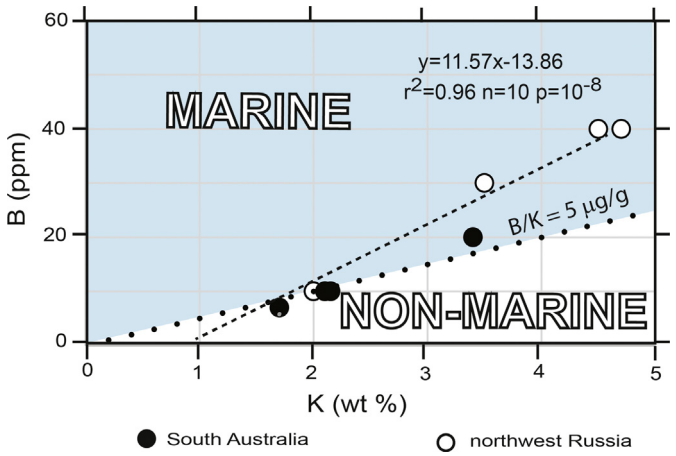

Fig. 9. B and K analyses of *Dickinsonia*, compared with marine rocks and paleosols from the same region (Table 1), and inferred marine-non-marine threshold of 5 µg/g B/K.

2011, 2012, 2013a). Mindi paleosols are gleyed and contain *Erytholus globosus* (of Table 1) below a stromatolitic limestone, and Madla paleosols include trace fossils such as *Skolithos linearis* (of Table 1), so both may have been marine influenced (Retallack, 2008). Tight covariance of B (ppm) and K (wt%), confirms that boron is carried largely by illlite clays (Frederickson and Reynolds, 1960).

Both fossils of *Dickinsonia* have low to undetectable boron as evidence of fresh or estuarine water during deposition of the rock layer overlying the fossil. Other marine fossils and silty paleosols from the same general regions are evidence for a cutoff between marine and non-marine deposition at 5 μg/g, though the differences between all these fossils are slight (Fig. 9). Calculated $\Delta_{B/K}$ values for both Weaver and Kübler indices independent of Ediacaran fossils (Eqs. (1) and (2)) of the matrix of *Dickinsonia*, *Erytholus*, and the Yaldati paleosol are negative, and thus non-marine. In contrast, positive values for *Skolithos*, *Vendotaenia*, *Yanischevskyites*, and *Platysolenites*, were more likely marine. Marine or non-marine discrimination by boron is within a standard error of Eqs. (3) and (4) for *Vendotaenia*, *Yanischevskyites*, and *Platysolenites*, so may not have been fully marine.

This study thus supports Pirrus (1992), who showed that Ediacaran vendobiont fragments like *Dickinsonia* and discoids (his plate 1, Figs. 1–2) from boreholes in Estonia were non-marine. His specimens had 42–72 ppm B in presumed freshwater shales and 97–228 ppm in presumed marine shale, for an 80 ppm cutoff, rather than 20 ppm cutoff for silty sandstones analyzed here. This difference can be attributed to the shallower burial and less diagenetic alteration of the samples of Pirrus (1992) on the western margin of the Baltic Basin. Pirrus (1992) did not provide potash assays or XRD traces, but Wichrowska (1982) found marine Vendian shales in Poland with mean B/K of only 24.1 ± 8.8 μg/g. Also proposed as freshwater are intertidal facies with *Dickinsonia tenuis* in the Konovalovka Subsuite of the Chernokamensk Suite in the Sylvitsa River, northwest of Yekaterinburg, Siberia (Grazhdankin et al., 2009, 2010; Bobkov et al., 2019). An X-ray diffractogram of Chernokamensk Formation (Grazhdankin et al., 2010) shows a broad illite peak with Weaver index 2.3 and Kübler index of 0.81. With a value of 33 ppm B and K_2O 3.37%, sample Us35 in underlying Perevalok Suite gives freshwater $\Delta_{B/K\text{-Weaver}} = -24$ and $\Delta_{B/K\text{-Kübler}} = -52$ μg/g. With 15 ppm B and K_2O 4.09%, sample Us-24 in the Chernokamensk Suite yields freshwater $\Delta_{B/K\text{-Weaver}} = -31$ and $\Delta_{B/K\text{-Kübler}} = -59$ μg/g. This Sylvitsa River occurrence is thus a fourth example of freshwater *Dickinsonia*, based on boron assay.

5.3. Continuing controversy on Dickinsonia

Dickinsonia in South Australia was traditionally interpreted as a shallow-marine creature of tidal flats, or thrown up in shores of coastal plains (Jenkins et al., 1983), but later facies analysis interpreted them as entirely submarine (Gehling, 2000). Comparable facies analysis of Russian *Dickinsonia* found them in middle to upper shoreface prodelta facies (Grazhdankin, 2004), and later in freshwater intertidal facies (Bobkov et al., 2019). Doubts about marine habitats came from the discovery of associated paleosols in South Australia, showing soil textures, hydrolytic weathering, carbonate nodules with pedogenic stable isotopic covariance, desert rose pseudomorphs, periglacial convolutions, and hydrolytic chemical weathering profiles (Retallack, 2013a, 2016a). Comparable periglacial soil deformation has also been found in Russia (Retallack, 2016a). Boron assay by itself does not discriminate paleosol, lake, estuary, or intertidal, only fully marine.

Motile marine animal interpretations of *Dickinsonia* rely on controversial “intermittent trails” of *Dickinsonia* (Ivantsov, 2013; Evans et al., 2019a, 2019b), which may instead be sessile individuals displaced by frost boils (Retallack, 2016a). Arcuate marginal lacerations and overfolds do not indicate current liftoff (Evans et al., 2015; Bobrovskiy et al., 2019), but demonstrate that *Dickinsonia* was attached to the bottom by forces greater than needed to tear the body apart (Retallack, 2017a). Narrow animal trails consuming immobilized *Dickinsonia* were considered scavenging of dead bodies (Gehling and Droser, 2018), but the trace fossils have lateral levees like surface trails of *Archaeonassa* (Buatois and Mángano, 2016), as indication that this was surface herbivory. Assemblages with *Dickinsonia* and other vendiobionts also show complex rank abundance distribution (Darroch et al., 2018), high β-diversity (Finnegan et al., 2019), and low interspecific interactions (Mitchell and Butterfield, 2018), unlike marine benthic communities, and more like terrestrial vegetation (Finnegan et al., 2019; Mitchell and Butterfield, 2018).

Preservation of *Dickinsonia* and other vendobionts is problematic because they show high relief, like plants or fungi with biopolymers such as cellulose and chitin (Retallack, 1994). The idea of rheological fill beneath a rigid carapace (Bobrovskiy et al., 2019) is falsified by lack of soft sediment deformation there, but chambered structure, in thin section (Retallack, 2016c). High relief was also supported by pyritization (Liu et al., 2019) or silicification (Tarhan et al., 2016), again like fossil plants. Cements of early silicification have Ge/Si ratios > 1 μmol/mol (Tarhan et al., 2016), characteristic of soil, not aquatic paleoenvironments (Retallack, 2017b). Dating by $^{234}U/^{238}U$ of iron oxides on some cover slabs (Tarhan et al., 2018) are an inadequate test for recent versus Ediacaran oxidation because the half-life of that rarely used isotopic system precludes an Ediacaran age. Alternating thick flagstones and thin laminae with *Dickinsonia* do not reflect alternating marine currents (Tarhan et al., 2017), but eolian drapes on flood-deposited flagstones (Retallack, 2019).

Shales with *Dickinsonia* in Russia lack the metazoan biomarker 24-isopropylcholesterane common in indisputably marine Ediacaran rocks of Oman and China (Pehr et al., 2018). Also in contrast with known Ediacaran marine rocks, Pehr et al. (2018) found that Russian shales have (1) unusually high and variable ratio of hopanes/steranes (1.6 to 119, thus variable but generally more bacteria than algae), (2) high and variable $\delta^{15}N$ (−2.8‰ outlier, mostly +3.5 to +6.5‰, thus generally without nitrate limitation); (3) high and variable $\delta^{13}Corg$ (−23.0 to −33.1‰, thus bacterial photosynthetic carbon-concentration mechanisms), and (4) low total organic carbon (0.09 to 1.06 wt%, thus highly oxidized). Biomarkers support the conclusion of Pirrus (1992) that eastern European Vendian shales were deposited in lakes or lagoons rather than oceans.

Cholestanes (C27) as remnants of cholesterol found in fossil *Dickinsonia* (Bobrovskiy et al., 2018) are not unique to animals, but widespread in red algae (Rhodophyta: Chardon-Loriaux et al., 1976), and many groups of fungi including Ascomycota (Kaneshiro and Wyder, 2000), Glomeromycota (Weete et al., 2010; Grandmougin-Ferjani et al., 1999), Zygomycota (Weete and Gandhi, 1997), and Chytridiomycota (Weete et al., 1989). This phylogenetic distribution suggests that cholesterol is basal to fungi and algae, and ergosterol (C28) evolved later (Weete et al., 1989; Gold, 2018). Fungal affinities for *Dickinsonia* may explain the declining ratios of stigmastane/cholestane in progressively larger and older specimens (Bobrovskiy et al., 2018). This would not be such a regular pattern if an animal were fouled in old age by green algae with stigmasterol (C29), but is compatible with long-term fungal growth from control of green algal symbionts.

While *Dickinsonia* as the first animal may be appealing (Bobrovskiy et al., 2019), alternative interpretation as a sessile lichenized fungus (Retallack, 1994, 2016c) has very different implications for the history of life. Likely terrestrial glomeromycotan fungi are known back to the Paleoproterozoic (Retallack et al., 2013a), well before known Ediacaran Glomeromycota (Yuan et al., 2005; Retallack, 2015c). The oldest undisputed animals are very different; small, tubular trace fossils (*Archaeonassa* of Buatois and Mángano, 2016) and body fossils (*Shanxilithes* of Meyer et al., 2012) of “Ediacaran Wormworld” (Schiffbauer et al., 2016). These trace and body fossils are also associated with Ediacaran Matresslands of vendobionts, and at least as geologically old as *Dickinsonia* (Gehling and Droser, 2018). These enigmatic small worms are more likely the oldest animals. Geochemical tools such as boron analysis now play a role in their interpretation.

6. Conclusions

This study adds evidence from boron that Ediacaran vendobionts were non-marine, in support of other evidence from paleosols, stable isotopes, mass balance geochemistry, birefringence fabrics, sand crystals, ice deformation, and tuff textures. The boron content of Ediacaran vendobionts is indistinguishable from that of fossil plants and paleosols, and significantly lower than that of known marine fossils, including Ediacaran stromatolites and algae. Unusually high in boron were paleosols with sulfate sand crystals, like those of modern acid sulfate lakes, and similar paleosols are common in Archean rocks. Precambrian thecamoebians, and the likely fungal fossil *Horodyskia* were freshwater. Unsurprising are marine salinities for trace fossils (*Skolithos*, *Manykodes*, *Lamonte*), problematica (*Conotubus*, *Palaeopasichnus*), algae (*Elainabella*, *Vendotaenia*, *Tenuocharta*, *Grypania*, and *Lanceoforma*). and microbes (*Eoleptonema*).

Declaration of competing interest

This is to confirm that I, Gregory J. Retallack, have no conflict of interest in researching and publishing the attached research manuscript "Boron paleosalinity proxy for deeply buried Paleozoic and Ediacaran fossils".

Acknowledgments

I thank Jeremy Retallack and Will Defliese for help during fieldwork. Allison Kirsch and Edward Davis aided in computer cataloguing of specimens into the Condon Collection. This project owes much to conversations with Dima Grazhdankin and Tom Algeo. This research was funded by a grant from the Sandal Society of the Museum of Natural and Cultural History of the University of Oregon.

References

Antcliffe, J.B., Gooday, A.J., Brasier, M.D., 2011. Testing the protozoan hypothesis for Ediacaran fossils: a developmental analysis of *Palaeopascichnus*. Palaeontology 54, 1157–1175.

Bebout, G.E., 2007. Metamorphic chemical geodynamics of subduction zones. Earth Planet. Sci. Lett. 260, 373–393.

Bobkov, N.I., Kolesnikov, A.V., Maslov, A.V., Grazhdankin, D.V., 2019. The occurrence of *Dickinsonia* in non-marine facies (La aparición de *Dickinsonia* en facies no marinas). Estud. Geol. 75, e096. https://doi.org/10.3989/egeol.43587.551.

Bobrovskiy, I., Hope, J.M., Ivantsov, A., Nettersheim, B.J., Hallmann, C., Brocks, J.J., 2018. Ancient steroids establish the Ediacaran fossil *Dickinsonia* as one of the earliest animals. Science 361, 1246–1249.

Bobrovskiy, I., Krasnova, A., Ivantsov, A., Luzhnaya (Serezhnikova), E., Brocks, J.J., 2019. Simple sediment rheology explains the Ediacara biota preservation. Nature Ecol. Evol. 3, 582–589.

Bottomley, D.J., Clark, I.D., 2004. Potassium and boron co-depletion in Canadian Shield brines: evidence for diagenetic interactions between marine brines and basin sediments. Chem. Geol. 203, 225–236.

Buatois, L.A., Mángano, M.G., 2016. Ediacaran ecosystems and the dawn of animals. In: Mángano, M.G., Buatois, L.A. (Eds.), The Trace-fossil Record of Major Evolutionary Events. v.1. Springer, Dordrecht, pp. 27–72.

Chardon-Loriaux, I., Morisaki, M., Ikekawa, N., 1976. Sterol profiles of red algae. Phytochemistry 15, 723–725.

Chetelat, B., Liu, C.Q., Gaillardet, J., Wang, Q.L., Zhao, Z.Q., Liang, C.S., Xiao, Y.K., 2009. Boron isotopes geochemistry of the Changjiang basin rivers. Geochim. Cosmochim. Acta 73, 6084–6097.

Couch, E.L., 1971. Calculation of paleosalinities from boron and clay mineral data. Amer. Assoc. Petrol. Geol. Bull. 55, 1829–1837.

Croghan, C., Egeghy, P.P., 2003. Methods of Dealing With Values Below the Limit of Detection Using SAS. 22. Southern SAS User Group, pp. 24–28.

Dalrymple, R.W., Narbonne, G.M., Smith, L., 1985. Eolian action and the distribution of Cambrian shales in North America. Geology 13, 607–610.

Darroch, S.A., Sperling, E.A., Boag, T.H., Racicot, R.A., Mason, S.J., Morgan, A.S., Tweedt, S., Myrow, P., Johnston, D.T., Erwin, D.H., Laflamme, M., 2015. Biotic replacement and mass extinction of the Ediacara biota. Proc. Roy. Soc, B 282, 20151003.

Darroch, S.A., Laflamme, M., Wagner, P.J., 2018. High ecological complexity in benthic Ediacaran communities. Nature Ecol. Evol. 2, 1541.

Dehler, C.M., Fanning, C.M., Link, P.K., Kingsbury, E.M., Rybczynski, D., 2010. Maximum depositional age and provenance of the Uinta Mountain Group and Big Cottonwood Formation, northern Utah: Paleogeography of rifting western Laurentia. Geol. Soc. Amer. Bull. 122, 1686–1699.

Dzik, J., 2005. Behavioral and anatomical unity of the earliest burrowing animals and the cause of the "Cambrian explosion". Paleobiology 31, 503–521.

Ercolani, C.P., 2018. Reconstruction of Modern and Past Weathering Regimes Using Boron Isotopes in River Sediments. Unpub. PhD thesis. University of Wollongong, Wollongong (332 p).

Ericson, D.B., Ewing, M., Wollin, G., Heezen, B.C., 1961. Atlantic deep-sea sediment cores. Geol. Soc. Amer. Bull. 72, 193–286.

Evans, S.D., Droser, M.L., Gehling, J.G., 2015. *Dickinsonia* liftoff: evidence of current derived morphologies. Palaeogeogr. Palaeoclim. Palaeoec. 434, 28–33.

Evans, S.D., Gehling, J.G., Droser, M.L., 2019a. Slime travelers: early evidence of animal mobility and feeding in an organic mat world. Geobiology 17, 490–509.

Evans, S.D., Huang, W., Gehling, J.G., Kisailus, D., Droser, M.L., 2019b. Stretched, mangled, and torn: responses of the Ediacaran fossil *Dickinsonia* to variable forces. Geology 47, 1049–1053.

Finnegan, S., Gehling, J.G., Droser, M.L., 2019. Unusually variable paleocommunity composition in the oldest metazoan fossil assemblages. Paleobiology 45, 1–11.

Fisher, A.T., Underwood, M.B., 1995. Calibration of an X-ray diffraction method to determine relative mineral abundances in bulk powders using matrix singular value decomposition: A test from the Barbados Accretionary Complex. In: Shipley, T.H., Ogawa, Y., Blum, P. (Eds.), Ocean Drilling Program, Initial Reports, Proceedings. 156. pp. 29–37.

Frederickson, A.F., Reynolds, R.C., 1960. Geochemical method for determining paleosalinity. In: Nat. Conf. Clays Clay Minerals Proc. 8. pp. 203–213.

Frey, M., 1987. Very low-grade metamorphism of clastic sedimentary rocks. In: Frey, M. (Ed.), Low Temperature Metamorphism. Blackie, Glasgow, pp. 9–58.

Fritz, G.B., Schill, R.O., Pfannkuchen, M., Brümmer, F., 2007. The freshwater jellyfish *Craspedacusta sowerbii* Lankester, 1880 (Limnomedusa: Olindiidae) in Germany, with a brief note on its nomenclature. J. Limnol. 66, 54–59.

Gehling, J.G., 2000. Environmental interpretation and a sequence stratigraphic framework for the terminal Proterozoic Ediacara Member within the Rawnsley Quartzite, South Australia. Precambrian Res. 100, 65–95.

Gehling, J.G., Droser, M.L., 2018. Ediacaran scavenging as a prelude to predation. Emerging Topics Life Sci 2, 213–222.

Gehling, J.G., Narbonne, G.M., Anderson, M.M., 2000. The first named Ediacaran body fossil, Aspidella terranovica. Palaeontology 43, 427–456.

Gold, D.A., 2018. The slow rise of complex life as revealed through biomarker genetics. Emerging Topics Life Sci 2, 191–199.

Goldberg, E.D., Arrhenius, G.O.S., 1958. Chemistry of Pacific pelagic sediments. Geochim. Cosmochim. Acta 13, 153–212.

Gorokhov, I.M., Felitsyn, S.B., Turchenko, T.L., Melnikov, N.N., Kutyavin, E.P., 2005. Mineralogy, geochemistry and isotopic geocheonology of Upper Venian shales from the Moscow Syneclise. Stratigr. Geol. Correl. 13, 476–494.

Grandmougin-Ferjani, A., Dalpé, Y., Hartmann, M.A., Laruelle, F., Sancholle, M., 1999. Sterol distribution in arbuscular mycorrhizal fungi. Phytochemistry 50, 1027–1031.

Grazhdankin, D., 2004. Patterns of distribution in the Ediacaran biotas: facies versus biogeography and evolution. Paleobiology 30, 203–221.

Grazhdankin, D.V., Bronnikov, A.A., 1997. A new locality of the remains of the late Vendian soft-bodied organisms on the Onega Peninsula. Doklady Akademia Nauk S.S.S.R 357, 792–796.

Grazhdankin, D., Gerdes, G., 2007. Ediacaran microbial colonies. Lethaia 40, 201–210.

Grazhdankin, D.V., Maslov, A.V., Krupenin, M.T., 2009. Structure and depositional history of the Vendian Sylvitsa Group in the western flank of the Central Urals. Stratigr. Geol. Correl. 17, 20–40.

Grazhdankin, D.V., Maslov, A.V., Krupenin, M.T., Ronkin, Y.L., 2010. Osadochnie Sistemi Sylvitskoi Serii (Verkhnii Vend Sredhego Urala) (Sedimentary Systems of the Sylvitsa Group (Upper Vendian of the Middle Urals)). Ural. Otd. Ross.Akad. Nauk, Yekaterinburg. pp. 1–277.

Grazhdankin, D.V., Goy, Y.Y., Maslov, A.V., 2012. Late Riphean microbial colonies adapted to desiccating environments. Dokl. Earth Sci. 446, 1157–1161.

Hall, M., Kaufman, A.J., Vickers-Rich, P., Ivantsov, A., Trusler, P., Linnemann, U., Hofmann, M., Elliott, D., Cui, H., Fedonkin, M., Hoffmann, K.H., 2013. Stratigraphy, palaeontology and geochemistry of the late Neoproterozoic Aar Member, southwest Namibia: reflecting environmental controls on Ediacara fossil preservation during the terminal Proterozoic in African Gondwana. Precambrian Res. 238, 214–232.

Hofer, G., 2009. Geochemische Untersuchungen an lakustrin-marinen Sedimenten der Bohrung Markgrafneusiedl T1 (Oberkreide, Gosau-Gruppe). Masters dissertation. University of Vienna (102 p).

Hofmann, H.J., 1985. Precambrian carbonaceous megafossils. In: Nitecki, M.H., Toomey, D.F. (Eds.), Paleoalgology. Springer, Berlin, pp. 20–33.

Horodyski, R.J., Mankiewicz, C., 1990. Possible Late Proterozoic skeletal algae from the Pahrump Group, Kingston Range, southeastern California. Amer. J. Sci. 290, 149–169.

Ishikawa, T., Nakamura, E., 1993. Boron isotope systematics of marine sediments. Earth Planet. Sci. Lett. 117, 567–580.

Ivantsov, A.Y., 2013. Trace fossils of Precambrian metazoans "Vendobionta" and "Mollusks". Stratigraphy Geological Correlation 21, 252–264.

Jenkins, R.J.F., Ford, C.H., Gehling, J.G., 1983. The Ediacara Member of the Rawnsley Quartzite: the context of the Ediacara assemblage (late Precambrian, Flinders Ranges). Geol. Soc. Australia J. 30, 101–119.

Jeong, J., McDowell, S.D., 2003. Characterization and transport of contaminated sediments in the southern Central Lake Superior. J. Minerals Materials Characteriz. Engineer. 2, 111–135.

Kaneshiro, E.S., Wyder, M.A., 2000. C27 to C32 sterols found in Pneumocystis, an opportunistic pathogen of immunocompromised mammals. Lipids 35, 317–324.

Keeley, J.A., Link, P.K., Fanning, C.M., Schmitz, M.D., 2013. Pre-to synglacial rift-related volcanism in the Neoproterozoic (Cryogenian) Pocatello Formation, SE Idaho: New SHRIMP and CA-ID-TIMS constraints. Lithosphere 5, 128–150.

Kennedy, M.J., Droser, M.L., 2011. Early Cambrian metazoans in fluvial environments, evidence of the non-marine Cambrian radiation. Geology 39, 583–586.

Kistler, R.B., Helvaci, C., 1994. Boron and borates. In: Industrial Minerals and Rocks. 6. pp. 171–186.

Liivamägi, S., Somelar, P., Mahaney, W.C., Kirs, J., Vircava, I., Kirsimäe, K., 2014. Late

Neoproterozoic Baltic paleosol: intense weathering at high latitude? Geology 42, 323–326.
Liivamägi, S., Somelar, P., Vircava, I., Mahaney, W.C., Kirs, J., Kirsimäe, K., 2015. Petrology, mineralogy and geochemical climofunctions of the Neoproterozoic Baltic paleosol. Precambrian Res. 256, 170–188.
Liu, A.G., McMahon, S., Matthews, J.J., Still, J.W., Brasier, A.T., 2019. Petrological evidence supports the death mask model for the preservation of Ediacaran soft-bodied organisms in South Australia. Geology 47, 215–218.
Mackereth, F.J.H., 1966. Some chemical observations on post-glacial lake sediments. Phil. Trans. Roy. Soc. London Biol. Sci. B 250, 165–213.
Maslov, A.V., Grazhdankin, D.V., Podkovyrov, V.N., Isherskaya, M.V., Krupenin, M.T., Petrov, G.A., Ronkin, Y.L., Gareev, E.Z., Lepikhina, O.P., 2009. Provenance composition and features of geological evolution of the Late Vendian foreland basin of the Timan orogen. Geochem. Int. 47, 1212–1233.
McIlroy, D., Green, O.R., Brasier, M.D., 2001. Palaeobiology and evolution of the earliest agglutinated Foraminifera: *Platysolenites*, *Spirosolenites* and related forms. Lethaia 34, 13–29.
Meyer, M., Schiffbauer, J.D., Xiao, S., Cai, Y., Hua, H., 2012. Taphonomy of the upper Ediacaran enigmatic ribbonlike fossil *Shaanxilithes*. Palaios 27, 354–372.
Meyer, M., Xiao, S., Gill, B.C., Schiffbauer, J.D., Chen, Z., Zhou, C., Yuan, X., 2014. Interactions between Ediacaran animals and microbial mats: insights from *Lamonte trevallis*, a new trace fossil from the Dengying Formation of South China. Palaeogeogr. Palaeoclim. Palaeoec. 396, 62–74.
Mitchell, E.G., Butterfield, N.J., 2018. Spatial analyses of Ediacaran communities at Mistaken Point. Paleobiology 44, 40–57.
Moran, A.E., Sisson, V.B., Leeman, W.L., 1992. Boron depletion during progressive metamorphism: implications for subduction processes. Earth Planet. Sci. Lett. 111, 331–349.
Murphy, C.P., 1983. Point counting pores and illuvial clay in thin section. Geoderma 31, 133–150.
Novoselov, A.A., de Souza Filho, C.R., 2015. Potassium metasomatism of Precambrian paleosols. Precambrian Res. 262, 67–83.
Nussman, D.G., 1965. Trace Elements in the Sediments of Lake Superior. Unpubl. PhD thesis. University of Michigan, Ann Arbor (243 p).
Pehr, K., Love, G.D., Kuznetsov, A., Podkovyrov, V., Junium, C.K., Shumlyanskyy, L., Sokur, T., Bekker, A., 2018. Ediacara biota flourished in oligotrophic and bacterially dominated marine environments across Baltica. Nature Communications 9, e 1807, 1–10.
Perry, E.A., 1972. Diagenesis and the validity of the boron paleosalinity technique. Amer. J. Sci. 272, 150–160.
Pirrus, E.A., 1992. Freshening of the late Vendian basin on the East European Craton. Estonian Acad. Sci. Geol. Proc. 41, 115–123.
Porter, S.M., Meisterfeld, R., Knoll, A.H., 2003. Vase-shaped microfossils from the Neoproterozoic Chuar Group, Grand Canyon: a classification guided by modern testate amoebae. J. Paleontol. 77, 409–429.
Retallack, G.J., 1994. Were the Ediacaran fossils lichens? Paleobiology 20, 523–544.
Retallack, G.J., 2000. Ordovician life on land and early Paleozoic global change. In: Gastaldo, R.A., DiMichele, W.A. (Eds.), Phanerozoic Ecosystems. Paleontological Society Papers. 6. pp. 21–45.
Retallack, G.J., 2001. *Scoyenia* burrows from Ordovician palaeosols of the Juniata Formation in Pennsylvania. Palaeontology 44, 209–235.
Retallack, G.J., 2008. Cambrian paleosols and landscapes of South Australia. Austral. J. Earth Sci. 55, 1083–1106.
Retallack, G.J., 2011. Problematic megafossils in Cambrian palaeosols of South Australia. Palaeontology 54, 1223–1242.
Retallack, G.J., 2012. Were Ediacaran siliciclastics of South Australia coastal or deep marine? Sedimentology 59, 1208–1236.
Retallack, G.J., 2013a. Ediacaran life on land. Nature 493, 89–92.
Retallack, G.J., 2013b. Early Cambrian humid, tropical paleosols from Montana. In: Driese, S.G., Nordt, L.E. (Eds.), New Frontiers in Paleopedology and Terrestrial Paleoclimatology. Soc. Econ. Paleont. Mineral. Spec. Pap. 44. pp. 257–272.
Retallack, G.J., 2015a. Reassessment of the Silurian problematicum *Rutgersella* as another post-Ediacaran vendobiont. Alcheringa 39, 573–588.
Retallack, G.J., 2015b. Late Ordovician glaciation initiated by early land plant evolution, and punctuated by greenhouse mass-extinctions. J. Geol. 123, 509–538.
Retallack, G.J., 2015c. Acritarch evidence of a late Precambrian adaptive radiation of Fungi. Botanica Pacifica 4, 19–33.
Retallack, G.J., 2016a. Field and laboratory tests for recognition of Ediacaran paleosols. Gondwana Res. 36, 94–110.
Retallack, G.J., 2016b. Ediacaran sedimentology and paleoecology of Newfoundland reconsidered. Sedimentary Geol 333, 15–31.
Retallack, G.J., 2016c. Ediacaran fossils in thin section. Alcheringa 40, 583–600.
Retallack, G.J., 2017a. Comment on: “Dickinsonia liftoff: evidence of current derived morphologies” by S. D. Evans, M. L. Droser, and J.G. Gehling. Palaeogeogr. Palaeoclim. Palaeoec. 485, 999–1001.
Retallack, G.J., 2017b. Exceptional preservation of soft-bodied Ediacara Biota promoted by silica-rich oceans: comment. Geology 44, e407.
Retallack, G.J., 2018a. Reassessment of the Devonian Problematicum *Protonympha* as another post Ediacaran vendobiont. Lethaia 51, 406–423.
Retallack, G.J., 2018b. Oldest recognized paleosols on Earth, Panorama Formation (3.46 Ga), Western Australia. Palaeogeogr. Palaeoclim. Palaeoec. 489, 230–248.
Retallack, G.J., 2019. Interflag sandstone laminae, a novel fluvial sedimentary structure with implication for Ediacaran paleoenvironments. Sediment. Geol. 379, 60–76.
Retallack, G.J., Mao, X., 2019. Paleoproterozoic (ca. 1.9 Ga) megascopic life on land in Western Australia. Palaeogeogr. Palaeoclim. Palaeoec. 532, 109266.
Retallack, G.J., Noffke, N., 2019. Are there ancient soils in the 3.7 Ga Isua Greenstone Belt, Greenland? Palaeogeogr. Palaeoclim. Palaeoec. 514, 18–30.
Retallack, G.J., Krull, E.S., Thackray, G.D., Parkinson, D., 2013a. Problematic urn-shaped fossils from a Paleoproterozoic (2.2 Ga) paleosol in South Africa. Precambrian Res. 235, 71–87.
Retallack, G.J., Dunn, K.L., Saxby, J., 2013b. Problematic Mesoproterozoic fossil *Horodyskia* from Glacier National Park, Montana, USA. Precambrian Res. 226, 125–142.
Retallack, G.J., Marconato, A., Osterhout, J.T., Watts, K.E., Bindeman, I.N., 2014. Revised Wonoka isotopic anomaly in South Australia and Late Ediacaran mass extinction. Geol. Soc. London J. 171, 709–722.
Retallack, G.J., Krinsley, D.H., Fischer, R., Razink, J.J., Langworthy, K., 2016. Archean coastal-plain paleosols and life on land. Gondwana Res. 40, 1–20.
Reynolds, R.C., 1965a. The concentration of boron in Precambrian seas. Geochim. Cosmochim. Acta 29, 1–16.
Reynolds, R.C., 1965b. Geochemical behavior of boron during the metamorphism of carbonate rocks. Geochim. Cosmochim. Acta 29, 1101–1114.
Rindsberg, A.K., Kopaska-Merkel, D.C., 2005. *Treptichnus* and *Arenicolites* from the Steven C. Minkin Paleozoic footprint site (Langsettian, Alabama, USA). In: Buta, R.J., Rindsberg, A.K., Kopaska-Merkel, D.C. (Eds.), Pennsylvanian Footprints in the Black Warrior Basin of Alabama. Mon. Alabama Paleont. Soc 1. pp. 121–141.
Rowland, S.M., Rodriguez, M.G., 2014. A multicellular alga with exceptional preservation from the Ediacaran of Nevada. J. Paleontol. 88, 263–268.
Schiffbauer, J.D., Huntley, J.W., O’Neil, G.R., Darroch, S.A., Laflamme, M., Cai, Y., 2016. The latest Ediacaran Wormworld fauna: setting the ecological stage for the Cambrian Explosion. GSA Today 26, 4–11.
Seilacher, A., 1992. Vendobionta and Psammocorallia: lost constructions of Precambrian evolution. Geol. Soc. London J. 149, 607–613.
Shirodkar, P.V., Dalal, V.K., 1988. Sediment boron and its relation to sediment properties in a tropical estuary. Mahasagar 21, 45–54.
Smith, E.F., Nelson, L.L., Strange, M.A., Eyster, A.E., Rowland, S.M., Schrag, D.P., Macdonald, F.A., 2016. The end of the Ediacaran: two new exceptionally preserved body fossil assemblages from Mount Dunfee, Nevada, USA. Geology 44, 911–914.
Spears, D.A., 1965. Boron in some British Carboniferous sedimentary rocks. Geochim. Cosmochim. Acta 29, 315–328.
Spears, D.A., Sezgin, H.I., 1985. Mineralogy and geochemistry of the Subcrenatum Marine Band and associated coal-bearing sediments, Langsett, South Yorkshire. J. Sediment. Res. 55, 570–578.
Środoń, J., Paszkowski, M., 2011. Role of clays in the diagenetic history of nitrogen and boron in the Carboniferous of Donbas (Ukraine). Clay Miner. 46, 561–582.
Tarhan, L.G., Hood, A.V., Droser, M.L., Gehling, J.G., Briggs, D.E., 2016. Exceptional preservation of soft-bodied Ediacara Biota promoted by silica-rich oceans. Geology 44, 951–954.
Tarhan, L.G., Droser, M.L., Gehling, J.G., Dzaugis, M.P., 2017. Microbial mat sandwiches and other anactualistic sedimentary features of the Ediacara Member (Rawnsley Quartzite, South Australia): implications for interpretation of the Ediacaran sedimentary record. Palaios 32, 181–194.
Tarhan, L.G., Planavsky, N.J., Wang, X., Bellefroid, E.J., Droser, M.L., Gehling, J.G., 2018. The late-stage “ferruginization” of the Ediacara Member (Rawnsley Quartzite, South Australia): Insights from uranium isotopes. Geobiology 16, 35–48.
Thompson, M.D., Ramezani, J., Crowley, J.L., 2014. U-Pb zircon geochronology of Roxbury Conglomerate, Boston Basin, Massachusetts: tectono-stratigraphic implications for Avalonia in and beyond SE New England. Amer. J. Sci. 314, 1009–1040.
Walker, C.T., Price, N.B., 1963. Departure curves for computing paleosalinity from boron in illites and shales. Amer. Ass. Petrol. Geol. Bull. 47, 833–841.
Walter, M.R., Oehler, J.H., Oehler, D.Z., 1976. Megascopic algae 1300 million years old from the Belt Supergroup, Montana: a reinterpretation of Walcott’s *Helminthoidichnites*. J. Paleontol. 50, 872–881.
Warr, L.N., Ferreiro Mählmann, R., 2015. Recommendations for Kübler index standardization. Clay Miner. 50, 283–286.
Weete, J.D., Gandhi, S.R., 1997. Sterols of the phylum Zygomycota: phylogenetic implications. Lipids 32, 1309–1316.
Weete, J.D., Fuller, M.S., Huang, M.Q., Gandhi, S., 1989. Fatty acids and sterols of selected hyphochytriomycetes and. Exper. Mycol. 13, 183–195.
Weete, J.D., Abril, M., Blackwell, M., 2010. Phylogenetic distribution of fungal sterols. PLoS One 5 (5), e10899.
Wei, H.Z., Jiang, S.Y., Tan, H.B., Zhang, W.J., Li, B.K., Yang, T.L., 2014. Boron isotope geochemistry of salt sediments from the Dongtai salt lake in Qaidam Basin: boron budget and sources. Chem. Geol. 380, 74–83.
Wei, W., Algeo, T.J., Lu, Y., Lu, Y., Liu, H., Zhang, S., Peng, L., Zhang, J., Chen, L., 2018. Identifying marine incursions into the Paleogene Bohai Bay Basin lake system in northeastern China. Int. J. Coal Geol. 200, 1–17.
Wichrowska, M., 1982. Bor w osadach ilastych górnego wendu lubelskiego skłonu platformy wschodnioeuropejskiej. Prz. Geol. 30, 230–234.
Williams, L.B., Hervig, R.L., 2005. Lithium and boron isotopes in illite-smectite: the importance of crystal size. Geochim. Cosmochim. Acta 69, 5705–5716.
Williams, L.B., Hervig, R.L., Holloway, J.R., Hutcheon, I., 2001. Boron isotope geochemistry during diagenesis. Part I. Experimental determination of fractionation during illitization of smectite. Geochim. Cosmochim. Acta 65, 1769–1782.
Ye, C., Yang, Y., Fang, X., Zhang, W., 2016. Late Eocene clay boron-derived paleosalinity in the Quaidam Basin and is implications for regional tectonics and climate. Sediment. Geol. 348, 49–59.
Yuan, X., Xiao, S., Taylor, T.N., 2005. Lichen-like symbiosis 600 million years ago. Science 308, 1017–1020.